Slit Discharge IR Spectroscopy of a Jet-Cooled Cyclopropyl Radical: Structure and Intramolecular Tunneling Dynamics†

Feng Dong, Scott Davis, and David J. Nesbitt*

JILA, National Institute of Standards and Technology and Department of Chemistry and Biochemistry, University of Colorado, Boulder, Colorado 80309

Received: July 19, 2005; In Final Form: August 24, 2005

High-resolution infrared spectra of a jet-cooled cyclopropyl radical are reported for the first time, specifically sampling the in-phase antisymmetric CH_2 stretch (ν_7) vibration. In addition to yielding the first precise gas-phase structural information, the spectra reveal quantum level doubling into lower (+) and upper (−) states due to tunneling of the lone α-CH with respect to the CCC plane. The bands clearly reveal intensity alternation due to H atom nuclear spin statistics (6:10 and 10:6 for even:odd K_a+K_c in lower (+) and upper (−) tunneling levels, respectively) consistent with C_{2v} symmetry of the cyclopropyl-tunneling transition state. The two *ground*-state-tunneling levels fit extremely well to a rigid asymmetric rotor Hamiltonian, but there is clear evidence for both local and global state mixing in the vibrationally *excited* ν_7 tunneling levels. In particular, the upper (−) tunneling component of the ν_7 state is split by anharmonic coupling with a nearly isoenergetic dark state, which thereby acquires oscillator strength via intensity sharing with this bright state. From thermal Boltzmann analysis of fractional populations, tunneling splittings for a cyclopropyl radical are estimated to be 3.2 ± 0.3 cm^{-1} and 4.9 ± 0.3 cm^{-1} in the ground and ν_7-excited states, respectively. This analysis indicates ground-state stereoracemization of the α-CH radical center to be a very fast process [$k \approx 2.0(4) \times 10^{11}$ s^{-1}], with the increase in the tunneling rate upon CH_2 in-phase asymmetric stretch excitation consistent with ab initio predictions of equilibrium vs transition-state zero-point energies. Modeling of the ground-state-tunneling splittings with high level ab initio 1D potentials indicates an improved $V_0 = 1115 \pm 35$ cm^{-1} barrier height for α-CH inversion through the cyclopropyl CCC plane.

I. Introduction

As highly reactive building blocks in organic synthesis, alkyl radicals play an important role in many processes, ranging from atmospheric chemistry[1] and combustion[2] through industrial synthesis in the petroleum and polymer industries[3,4] to molecular synthesis in the interstellar medium.[5] By virtue of their extreme reactivity, however, radical concentrations are typically vanishingly small under steady-state conditions. A detailed study of radical spectroscopic properties thus represents an ongoing experimental challenge, demanding much more sensitive and sophisticated detection methods than those required for stable closed-shell molecules. The resulting rewards for such efforts, however, are significant. For example, the capability for quantum state-resolved spectroscopy and detection of these radicals enables detailed real-time studies of kinetics to be pursued under controlled laboratory conditions. Of particular importance in this regard have been high-resolution IR spectroscopic methods, which offer nonintrusive quantum state-resolved access to radical concentrations even in chemically complex gas-phase reaction mixtures such as are routinely encountered in a combustion environment.

As a result of this interest, experimental methods have been developed for the IR spectroscopic studies of radicals, starting with the pioneering flash kinetic IR spectroscopy efforts of Pimentel and co-workers.[6] These early direct absorption methods have been greatly extended in spectral resolution, sensitivity, and spectral brightness with tunable IR lasers, permitting access to several polyatomic radicals generated by pulsed UV photolysis of suitable precursor molecules in a laser multipass flow cell. However, because of broad Boltzmann populations at room temperature and consequent thermal dilution of molecules per quantum states, these methods have been limited to relatively small polyatomic radical species under room temperature conditions. For species important in combustion, this can be quite limiting and, in particular for hydrocarbons, has restricted applications to relatively small alkyl transients such as methyl,[7] vinyl,[8] ethyl,[9] allyl,[10] and propargyl radicals.[11]

A major sensitivity improvement in these methods is obtained by the combination of IR laser absorption with supersonic jet cooling, as implemented both by slit discharge or UV photolysis generation of the desired radical species.[12−18] The principal advantages of jet cooling are 2-fold: (i) radicals are concentrated mostly in the lowest quantum levels, thus increasing the population per quantum state, and (ii) spectral congestion is substantially reduced. This latter restriction becomes more significant with an increasing number of C atoms. Indeed, spectra of polyatomic species even as "simple" as ethyl and allyl radicals are sufficiently complicated under room temperature conditions that their assignment has been greatly facilitated by spectroscopic studies under jet-cooled conditions.[13,16,17] Nevertheless, it is fair to say that this powerful combination of jet cooling and "universal" spectroscopic detection by direct IR laser absorption is still in its relatively early stages and therefore represents both a challenging, promising, area of research.

† Part of the special issue "Jürgen Troe Festschrift".

* To whom correspondence should be addressed: e-mail: djn@jila.colorado.edu.

10.1021/jp053994u CCC: $33.50
Published on Web 11/03/2005

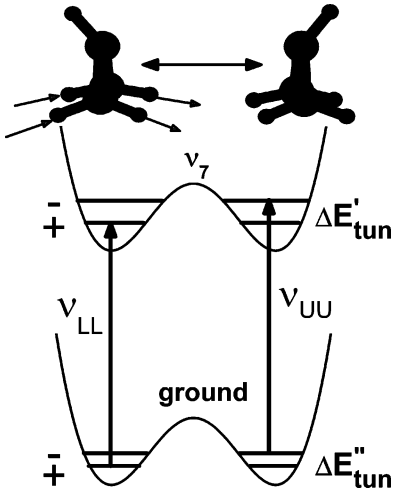

Figure 1. Illustration of double-minimum potentials for the ground and excited states (ν_7) of cyclopropyl radical. According to symmetry considerations and nuclear spin statistics (see Table 1), only two transitions with nonzero oscillator strength are allowed, i.e., c-type bands for $\nu_7^+ \leftarrow 0^+$ and $\nu_7^- \leftarrow 0^-$, which give only the *difference* of the ground- and excited-state tunneling splittings.

One polyatomic open-shell species of particular interest is the cyclopropyl radical, which has been of long-standing interest in both synthetic organic chemistry and chemical physics. First it is the simplest cyclic hydrocarbon radical and a prototype for homolytic cleavage of the β-CC bond. Indeed, the CCC ring in a cyclopropyl radical leads to energetically unfavorable bond angles, providing a benchmark for hydrocarbon strain effects[19] in open shell systems small enough for both experimental[20−33] and theoretical[34−40] studies. Second, as illustrated in Figure 1, the α-C radical center is nominally sp^3 hybridized, leading to a familiar double-well potential for transfer of the α-H atom across the CCC plane. Though classically inaccessible from the ground state at the planar HCCC transition-state configuration, this double-well potential nevertheless results in rapid quantum tunneling from one minimum to the other. This tunneling represents an elementary prototype for stereochemistry around a hydrocarbon radical center, the retention or inversion of which for asymmetrically substituted cyclopropyl species is critical in *chiral* organic and pharmaceutical synthesis pathways.[41] Finally, the C_3H_5 radical can exist in multiple isomeric forms and thus serves as a testbed for the important dynamics of chemical isomerization in open shell combustion species. For example, it can cleave the β-CC bond to form the energetically more stable allyl radical ($\Delta H^0 \approx -22$ kcal/mol). The barrier heights and dynamics of such symmetry-forbidden electrocyclic ring-opening reactions have remained a source of controversy for decades.[33,39,42−48]

Spectroscopically, the first successful detection of a cyclopropyl radical was obtained via electron spin resonance spectroscopy (ESR), resulting in nuclear hyperfine measurements for both H and ^{13}C substituted atoms.[20] Early insights into the large amplitude dynamics of a cyclopropyl radical were extracted from these condensed phase spectra simply by interpreting nuclear hyperfine parameters in terms of *expectation values* of the Hamiltonian averaged over the tunneling inversion coordinate. Later ESR studies by Kochi and co-workers[49] revealed the hyperfine interactions between syn and anti β-H atoms in the CH_2 groups to be identical. This equivalence is consistent with a true C_{2v} equilibrium geometry (i.e., α-CH in the CCC plane) but could also arise dynamically as a result of fast tunneling between equivalent C_s structures (i.e., α-CH out of the CCC-plane) through a C_{2v} transition state. The first vibrational information on a cyclopropyl radical was obtained by Dyke and co-workers,[23] who measured photoelectron spectra and assigned the α-CH bending mode at the carbon radical center to 1000 ± 70 cm^{-1} from analysis of the band structure. The only direct IR measurement of cyclopropyl vibrational frequencies to date comes from matrix-isolation studies by Holtzhauer and co-workers.[45] Interestingly, the cyclopropyl radical in these studies was produced by the photochemical electrocyclization of allyl radical in the matrix, which, despite being strongly *endothermic* from the ground state, can be made to occur rapidly via electronic excitation. Although spectral resolution was limited by matrix shifts and broadening due to the condensed phase environment, 16 bands were observed and tentatively assigned to cyclopropyl vibrations with the aid of ab initio frequency calculations. Furthermore, by comparison of experimental and ab initio frequency predictions for the C_s and C_{2v} geometries, the authors used the data to support an out-of-plane α-CH equilibrium structure.

Substantial theoretical efforts have also been directed toward a cyclopropyl radical, specifically in order to elucidate ESR spectra[40] and predict harmonic vibrational frequencies and equilibrium structures. There is now a general ab initio consensus for a C_s equilibrium geometry, with a double minimum potential for α-CH motion across a C_{2v} transition state. Calculations at a modest level of theory [QCISD(T)/DZP] predict the reaction path for α-CH inversion to have a 3.7 kcal/mol (≈1280 cm^{-1}) barrier, with tunneling splittings along an effective vibrationally adiabatic 1D reaction path[40] calculated to be 1.1 cm^{-1} for the ground state, i.e., readily detectable via high-resolution methods. As shown later in this paper, such calculations can be substantially improved; nevertheless, these theoretical estimates provide a useful starting point for guiding our search for tunneling dynamics in the present spectra.

Cyclopropyl radical also exhibits other interesting unimolecular dynamics; specifically, interconversion between cyclopropyl and allyl radicals has been studied both experimentally and theoretically for several decades. Allyl radical is energetically more favorable by $\Delta H^0 \approx -22$ kcal/mol, suggesting ring strain effects in the cyclopropyl radical that promote rapid fission of the β-CC bond.[24] However, large barriers to such exothermic processes arise in such electrocyclic reactions from orbital symmetry conservation, as first developed by Woodward and Hoffmann.[46] Indeed, Longuet-Higgins and Abrahamson[47] concluded that the conversion of a cyclopropyl into an allyl radical is "forbidden" by orbital analysis and state correlation diagrams and thus predicted a large activation energy for β-CC fission. Although this prediction is clearly consistent with experimental evidence for a stable cyclopropyl radical, conversion in both directions between cyclopropyl and allyl has been observed experimentally. For example, by measuring cyclopropane and propylene production by reaction of a CH_3 radical with cyclopropane-carboxaldehyde at 40−80 Torr and 100−200 °C, Greig and Thynne[24,25] deduced that an allyl could be formed either thermally by isomerization from a cyclopropyl radical or by decomposition of some high-energy methyl cyclopropyl radical or methylcyclopropane, with a ≈10% conversion efficiency reported at 174 °C. However, the possibility of direct isomerization of cyclopropane to propylene could not be excluded. Conversely, the matrix spectroscopy studies of Holtzhauer and co-workers[45] were based on cyclopropyl radicals being *formed* by the cyclization of an allyl in photochemically excited states. Despite the strong evidence for isomer interconversion, the magnitude of the ground-state dissociation barrier to β-CC fission as well as an explicit mechanism for ring

opening or closing (i.e., either by "conrotatory" or "disrotatory" twisting of the CH_2 groups with respect to the CCC plane) still remain controversial issues.[33,39,43,44,48]

The focus of this paper is high-resolution near-IR spectroscopy of a jet-cooled cyclopropyl radical generated by dissociative electron attachment of cyclopropyl bromide in the throat of a slit supersonic discharge and monitored by direct absorption of tunable high-resolution IR laser radiation in the C−H stretch region. This is the first such report of high-resolution gas-phase spectra and thus provides novel opportunities for direct comparison with theory, both in terms of equilibrium structure and large-amplitude tunneling-sampling regions near the transition state. Furthermore, with the help of prior IR spectroscopy in the C−H stretch region,[17,50−52] these studies also permit direct measurement of the small, but finite, allyl vs cyclopropyl branching ratios in the discharge. This measurement testifies to the remarkably "gentle" nature of the discharge environment as well as providing insight into the dynamics of electron dissociative attachment to the cyclopropyl halide.

The rest of this paper is organized as follows. A description of the slit-jet discharge high-resolution IR spectrometer is briefly discussed in section II. Spectroscopic background relevant to cyclopropyl is presented in section III, with experimental results and data analysis reported in section IV for the in-phase antisymmetric CH_2-stretch vibration (ν_7). Of special dynamical interest, three overlapping vibrational bands are observed for what should be an isolated C−H stretch. One pair of bands can be explained by tunneling splittings, which serve as a sensitive probe of barrier height to α-CH stereoisomerization across the CCC plane. However, the presence of a third band arises from anharmonic coupling between the optically allowed ν_7 ("bright") state and an optically inactive ("dark") state at nearly isoenergetic energy, which will be presented in section V along with the first precise gas-phase structural information for this radical. Also in section V, detection of the allyl isomer radical in the jet is discussed, providing evidence for a small but finite (≈7%) ring-opening channel in the dissociative electron attachment formation of a cyclopropyl radical. The main results and conclusions of the paper are summarized in section VI.

II. Experiment

Cyclopropyl radical spectra are obtained with a high-resolution infrared slit-jet discharge spectrometer apparatus presented in detail elsewhere.[53−55] Tunable infrared light (from 2500 to 5000 cm^{-1}, typically ≈35 μW around 3050 cm^{-1}) is generated via difference-frequency generation of two visible cw lasers, a single-mode Ar^+ laser (514 nm), and a tunable ring dye laser (R6G) by collinearly passing through a periodically poled $LiNbO_3$ (PPLN) crystal. The infrared light is split into signal and reference beams after the PPLN and monitored separately on two matched InSb photovoltaic detectors. By fast electronic subtraction of the signal and reference beams, common mode noise can be reduced to near shot-noise-limited levels (≈6×10^{-5} in a 10 kHz detection bandwidth). Before reaching the detector, the signal beam traverses the 4 cm long, 300 μm slit jet in a 16-pass Herriot cell configuration, that increases the absorption length to 64 cm. Signals are then detected in the time domain by transient differential absorptions synchronous with the slit valve pulse. Ar^+ laser frequency stability (<2 MHz) is maintained by locking to a 30 cm long optical transfer cavity, which, in turn, achieves absolute frequency precision by active stabilization on a polarization-stabilized HeNe laser. Dye laser frequency stability (<2 MHz) and tuning are maintained by servo loop control onto a separate Fabry-Perot cavity, with the IR difference frequency directly measured via transmission fringes on the fixed frequency optical transfer cavity.[56]

TABLE 1: Vibration and Rotation Symmetries of Cyclopropyl Radical According to the Molecular Symmetry Group C_{2v}(M)[a]

	E E	C_2 (12)	σ_{ab} E*	$\sigma_\perp$ (12)*	transition dipole moment	vibration symmetry	rotation symmetry (statistical weight) 0^+	 0^-
A_1	1	1	1	1	μ_b	0^+, ν_7^-, ν_1^+, ν_2^+	ee (6)	ee (10)
A_2	1	1	−1	−1			oo (6)	oo (10)
B_1	1	−1	−1	1	μ_c	0^-, ν_7^+, ν_1^-, ν_2^-	eo (10)	eo (6)
B_2	1	−1	1	−1	μ_a		oe (10)	oe (6)

[a] In the in-phase antisymmetric CH_2 stretch region (ν_7), only two transitions with nonvanishing oscillator strength ($\langle\nu_7^+|\mu_c|0^+\rangle$ and $\langle\nu_7^-|\mu_c|0^-\rangle$) are allowed. The nuclear spin statistical weights are also included.

High densities of rotationally cold cyclopropyl radical are generated by a 500 V 0.7 A pulsed discharge through a pulsed mixture of 0.5% cyclopropyl bromide in 70% Ne/30% He at a stagnation pressure of 500 Torr. Radical concentrations are square-wave modulated at 50 kHz, with the lock-in detection of the absorbance signals yielding absorbance sensitivities of 6×10^{-7} $Hz^{-1/2}$ (6×10^{-5} absorbance in a 10 kHz bandwidth) and provide excellent discrimination against precursor molecules present in orders of magnitude higher concentrations. Relative frequencies are obtained with ≈10 MHz precision (≈0.0003 cm^{-1}) via fringe interpolation on the optical transfer cavity, with an absolute infrared frequency reference to the CH_4 R(0) transition at 3028.7528 cm^{-1}.[57]

III. Spectroscopic Background

Tunneling of the α-CH between the two C_s equilibrium geometries is a feasible large-amplitude process at our spectral resolution, requiring consideration of permutation-inversion molecular symmetry.[58] As a result of such tunneling, the pairs of anti-H atoms in the two CH_2 groups are equivalent, and thus the cyclopropyl radical can be shown to transform according to the C_{2v}(M) molecular symmetry group. The corresponding symmetries in this group for the dipole moment vector (μ_a,μ_b,μ_c), vibrations, and rotations (J_{KaKc}) can be readily evaluated, as summarized in Table 1. Each rovibrational state is doubled, with symmetric (+) and antisymmetric (−) labels for the lower and upper tunneling states, respectively. Nuclear spin statistics, due to feasible exchange of each of the two pairs of identical anti-H atoms ($I_H = 1/2$) in the two CH_2 groups, can also be readily predicted from MS group theory. This procedure yields 6:10 nuclear spin weights for the totally symmetric lower tunneling state (0^+) and 10:6 for the upper tunneling state (0^-) for rotational states with $K_a + K_c$ = even (e): $K_a + K_c$ = odd (o), respectively.

In combination with symmetry considerations for the lower/upper tunneling (±) and corresponding vibrational wave functions, the allowed transitions with nonvanishing oscillator strengths in the C−H stretch region can be easily identified. Although the predicted intensity is relatively weak (1.0×10^{-18} cm/molecule for the ν_1 band and 3.3×10^{-18} cm/molecule for the ν_7 band), the α-CH stretch (ν_1) would be the optimal choice for spectroscopic measurement of tunneling splittings since all four transitions have nonvanishing oscillator strengths (i.e., $\langle\nu_1^+|\mu_b|0^+\rangle$, $\langle\nu_1^+|\mu_c|0^-\rangle$, $\langle\nu_1^-|\mu_c|0^+\rangle$, and $\langle\nu_1^-|\mu_b|0^-\rangle$ are all nonzero). A similar case was exploited in recent studies[59,60] of isotopically substituted HD_2O^+, where the C_{2v}(M) vs D_{3h}(M) symmetry breaking of the partially deuterated species away from

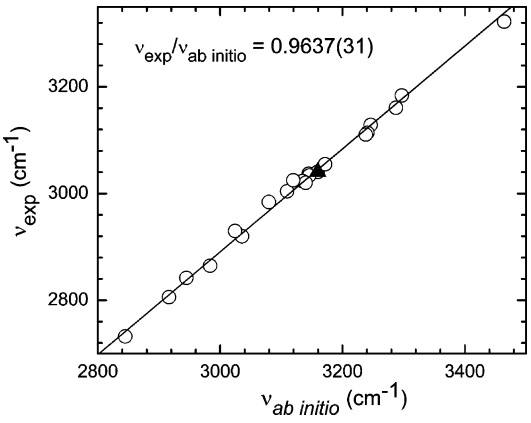

Figure 2. Frequency correlation between ab initio harmonic frequencies [B3LYP/6-311++G(3df,3pd)] and experimentally observed frequencies for the C−H stretches in hydrocarbon radicals. The well-fitted linear feature gives the scaling factor $\nu_{exp}/\nu_{ab\ initio} = 0.9637(31)$ and the 10 cm^{-1} standard deviation at the 3000 cm^{-1} region which is used to guide the experiment. The solid triangle is the experimental result for the ν_7 in-phase antisymmetric stretch of cyclopropyl radical, which is ≈3.5 cm^{-1} lower than the predicted frequency (3045 cm^{-1}) for the $\nu_7^+ \leftarrow 0^+$.

H_3O^+ and D_3O^+ permits observation of both the *sum* and *difference* of the ground- and excited-state tunneling splittings from a *single* vibrational manifold. However, ab initio calculations (vide infra) predict this α-CH stretch (ν_1) band to overlap known strong vibrations of the cyclopropyl bromide precursor present in much higher densities. Therefore, despite considerable suppression of precursor absorption offered by concentration modulation methods, this makes the α-CH stretch band less attractive for initial high-resolution spectral investigations.

Alternatively, the in-phase asymmetric CH_2 stretch (ν_7) exhibits a greatly reduced overlap between its precursor and the highest predicted infrared intensities in the accessible laser region. There are only two allowed transitions with nonzero oscillator strength, i.e., $\langle \nu_7^+|\mu_c|0^+\rangle$ and $\langle \nu_7^-|\mu_c|0^-\rangle$. As shown in Figure 1, these two bands do not bridge the tunneling gap and will exhibit a C-type rotational band structure. As a result, these "lower ← lower" and "upper ← upper" transitions provide information on the *difference* ($\Delta E_{tun}' - \Delta E_{tun}''$) in tunneling splittings between the upper and lower vibrational manifolds. However, the ground-state tunneling splitting can still be reliably estimated by precise intensity ratios for transitions out of the 0^+ and 0^- states, as has been demonstrated to be remarkably accurate for the HD_2O^+ system.[60] For a typical cyclopropyl radical concentration (10^{12} radicals/cm^3), rotational temperature (20 K), and ν_7-integrated band strength ($S_{pred} = 3.32 \times 10^{-18}$ cm/radical), peak absorbance should be ≈0.25%, which at our sensitivity translates into an acceptable *S*/*N* ratio of ≈40.

In this paper, high-resolution infrared spectra of cyclopropyl radical sampling in-phase antisymmetric CH_2 stretch excitation are reported. To achieve efficient scanning at high spectral resolution, ab initio predictions of vibrational frequencies prove essential but only when suitably benchmarked against known radical spectra. By way of example, Figure 2 displays a frequency correlation between the *calculated harmonic* frequencies [B3LYP/6-311++G(3df,3pd)] and *experimentally measured* fundamental frequencies for all known C−H stretch vibrations in hydrocarbon radicals. As expected, the correlation is extremely good and provides a calibrated linear scaling factor of $\nu_{exp}/\nu_{ab\ initio} = 0.9637(31)$. Of even greater importance, however, the tight clustering and small scatter in this combined experimental/theoretical plot indicate a ≈10 cm^{-1} standard deviation in the 3000 cm^{-1} region, which already represents a manageable near-IR search even at high resolution. Based on B3LYP/6-311++G(3df,3pd) calculations for a cyclopropyl radical, the ν_7 band origin is predicted to occur at 3045 ± 10 cm^{-1}, as denoted by the triangle in Figure 2. Indeed, the experimentally observed and deperturbed $\nu_7^{\pm} \leftarrow 0^{\pm}$ band origins reported herein prove in very good agreement with these predictions (3040.7 and 3042.4 cm^{-1}), i.e., both are well within the estimated $\sigma \approx 10$ cm^{-1} uncertainty. This quality of successful prediction has been confirmed for several other benchmark hydrocarbon radicals and molecular ions,[13,15,17,59−63] which bodes well for studies of even more complex radical systems.

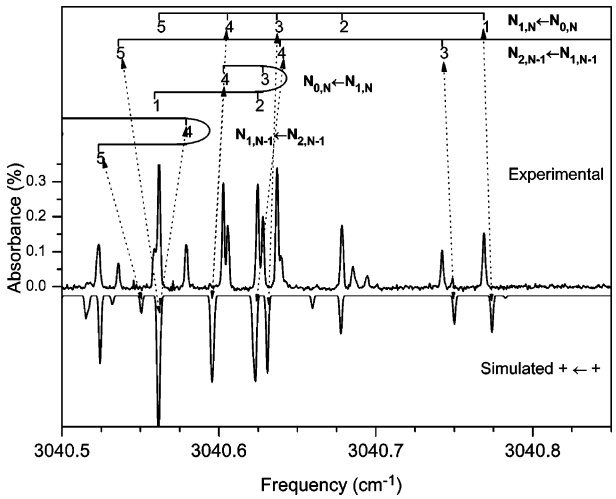

Figure 3. An experimental Q-branch observed in the predicted in-phase antisymmetric CH_2 stretch (ν_7) region of cyclopropyl radical and the corresponding calculated spectrum and the assignment. This band is assigned to the $\nu_7^+ \leftarrow 0^+$ with the aid of nuclear spin statistics, as shown in Figure 4. While all of the ground state two-line combination differences are well fit to a Watson asymmetric Hamiltonian, some lines have been strongly pushed away from the predicted position (dotted lines), indicating large perturbations in the excited state but not the ground state.

IV. Results and Analysis

With several strong transitions from a cyclopropyl radical positively identified, experimental conditions are then reoptimized and the scan range expanded to cover the full spectral region. This process reveals several vibrational bands that can be assigned to transitions out of either the lower (i.e., $\nu_7^+ \leftarrow 0^+$) or upper (i.e., $\nu_7^- \leftarrow 0^-$) tunneling levels, as reported below.

A. $\nu_7^+ \leftarrow 0^+$ Band ("Lower ← Lower"). The first C−H stretch band due to a cyclopropyl radical is observed near 3040.6 cm^{-1}, ≈4.5 cm^{-1} below the scaled harmonic frequency prediction for ν_7. The spectrum exhibits clear P, Q, and R branch structures characteristic of a c-type band and is consistent with expectations for the in-phase antisymmetric stretch. A sample 0.4 cm^{-1} scan region over the central Q-branch feature is shown in Figure 3 along with the corresponding spectral simulation from the full least-squares fit described below.

Via standard spectroscopic analysis, 15 four-line ground-state combination difference pairs can be rigorously identified from the P, Q, and R branch progressions, as shown in Table 2, where $J'K_a'K_c'$ are the rotational quantum numbers in the excited state and $J''K_a''K_c''$ are those in the ground state. The standard deviation for all of these four-line combination differences is ≈9 MHz; this can be used to make preliminary fits and extract term values with which to make more assignments based on

TABLE 2: Measured Four-Line Ground-State Combination Differences (C.D.) and Corresponding Transition Frequencies for the $\nu_7^+ \leftarrow 0^+$ (Lower ← Lower) Band of Cyclopropyl Radical[a]

$J'K_a'K_c'$	$J''K_a''K_c''$ (1)	ν_1 (cm^{-1})	$J''K_a''K_c''$ (2)	ν_2 (cm^{-1})	C.D. (cm^{-1})	obs-pred (10^{-4} cm^{-1})
2 2 1	2 1 1	3040.9680	1 1 1	3043.7258	2.7578	−4.9
1 0 1	2 1 1	3037.8007	1 1 1	3040.5590	2.7583	0.0
2 1 1	2 2 1	3040.3378	1 0 1	3043.5067	3.1689	−9.2
1 1 1	2 2 1	3037.5993	1 0 1	3040.7690	3.1697	−1.7
3 3 1	3 2 1	3041.2614	2 2 1	3045.2633	4.0019	2.4
2 1 1	3 2 1	3036.3355	2 2 1	3040.3378	4.0023	6.8
3 2 2	3 1 2	3040.7423	2 1 2	3045.0680	4.3257	−3.0
2 0 2	3 1 2	3036.2988	2 1 2	3040.6247	4.3259	−1.4
3 1 2	3 2 2	3040.4971	2 0 2	3044.9684	4.4713	−1.2
2 1 2	3 2 2	3036.2070	2 0 2	3040.6784	4.4714	−0.1
2 2 1	3 3 1	3036.0441	2 1 1	3040.9680	4.9239	4.0
3 2 1	3 3 1	3040.0065	2 1 1	3044.9306	4.9241	6.2
4 3 2	4 2 2	3040.9239	3 2 2	3046.5561	5.6322	−4.6
3 1 2	4 2 2	3034.8643	3 2 2	3040.4971	5.6328	1.4
3 0 3	4 1 3	3034.7704	3 1 3	3040.6280	5.8576	4.3
4 2 3	4 1 3	3040.6388	3 1 3	3046.4967	5.8579	7.5
3 1 3	4 2 3	3034.7476	3 0 3	3040.6370	5.8894	−1.1
4 1 3	4 2 3	3040.5792	3 0 3	3046.4687	5.8895	0.3
4 2 2	4 3 2	3040.2537	3 1 2	3046.3203	6.0666	−7.7
3 2 2	4 3 2	3034.6746	3 1 2	3040.7423	6.0677	3.6
4 3 1	4 4 1	3039.5913	3 2 1	3046.3791	6.7878	−2.6
3 3 1	4 4 1	3034.4732	3 2 1	3041.2614	6.7882	0.8
5 4 2	5 3 2	3041.1929	4 3 2	3048.0394	6.8465	0.5
4 2 2	5 3 2	3033.4069	4 3 2	3040.2537	6.8468	4.1
4 1 3	5 2 3	3033.3289	4 2 3	3040.5792	7.2503	−1.7
5 3 3	5 2 3	3040.6855	4 2 3	3047.9358	7.2503	−1.3
4 2 3	5 3 3	3033.2568	4 1 3	3040.6388	7.3820	−3.4
5 2 3	5 3 3	3040.4603	4 1 3	3047.8433	7.3830	5.9
4 3 2	5 4 2	3033.1430	4 2 2	3040.9239	7.7809	1.4
5 3 2	5 4 2	3039.8755	4 2 2	3047.6565	7.7810	2.2

[a] All 38 ground-state two-line combination differences from 71 IR transitions can be well fit to a Watson asymmetric Hamiltonian (A-reduction, IIIr-representation, $\sigma = 0.00032$ cm^{-1}).

ground-state two-line combination differences. A total of 71 lines are thus unambiguously assigned. From this complete data set, 37 two-line combination differences are extracted for the ground state and fit to a Watson asymmetric top Hamiltonian (A-reduction, IIIr-representation). The standard deviation of the fit is ≈10 MHz, which is consistent with our measurement precision and indicates a lack of perturbation in the lower state. Rotational constants from this fully unperturbed fit are summarized in Table 4 and provide high quality input that will be used later to extract structural information for cyclopropyl radical (see section V).

One can also make an unambiguous assignment of this band to transitions out of the ground-state lower (+) tunneling level by examining nuclear spin intensity alternation, as mentioned previously. Specifically, Figure 4 shows an experimental sample R branch spectral region for this vibrational band and two predicted spectra for the two cases of 6:10 (+ ← +) and 10:6 (− ← −) nuclear spin weights for $K_a + K_c$ = even:odd. Comparison with the observed spectrum makes it quite clear that this band follows the 6:10 (+ ← +) spin weights and thus can be assigned to transitions out of the lower tunneling state, i.e., $\nu_7^+ \leftarrow 0^+$.

In contrast to the high quality of these ground-state asymmetric-top fits, the corresponding upper ($\nu_7 = 1$) state shows evidence of perturbations. This is easily seen in the experimental vs simulated Q branch spectral region in Figure 3, where the dotted arrows designate frequency discrepancies for some of the most strongly perturbed upper states. These discrepancies indicate individual line shifts of up to ≈0.030 cm^{-1}, i.e., more than 2 orders of magnitude in excess of the experimental uncertainty, but not so large as to inhibit an unambiguous assignment. These line shifts imply the presence of strong local interactions between isolated rotational levels of ν_7^+ and some dark-state manifold (or manifolds), with coupling matrix elements at least on the order of $\beta \approx 0.030$ cm^{-1}. Indeed, this coupling is confirmed by analysis of even stronger dark-state interactions in the ν_7^- upper state, as shown below. We will return to this later in the discussion, but for the moment present results from a least-squares Watson asymmetric analysis of the full band, holding the ground-state constants fixed at the values determined above. As the upper-state perturbations are small but ubiquitous, we choose to fit only to a rigid model for the upper state. The results are also summarized in Table 4. The fit to rigid rotor A, B, and C constants is very good, although the standard deviation ($\sigma \approx 360$ MHz) is much higher than that of the ground state and cannot be significantly improved by inclusion of centrifugal terms. It can be improved by sequential exclusion of the less well-predicted lines; however, this process converges slowly, suggesting a weak, but pervasive, level of coupling of nearly all levels with background vibrational states.

B. $\nu_7^- \leftarrow 0^-$ Band ("Upper ← Upper"). The tunneling splitting due to α-CH bending in a cyclopropyl radical is predicted[40] to be between ≈1 and 10 cm^{-1}, i.e., the same order of thermal energy as in the discharge expansion. Thus one expects a second vibrational band due to $\nu_7^- \leftarrow 0^-$ ("upper ← upper") with an intensity diminished by thermal population of the first excited tunneling state (0^-). We do indeed observe such additional band structure, as signaled by an intense Q-branch structure ≈1.5 cm^{-1} to the blue of the $\nu_7^+ \leftarrow 0^+$ band origin (Figure 5). Surprisingly, however, there are clearly *two* such Q-branches separated by ≈0.44 cm^{-1}, with the high- and low-frequency bands labeled (a) and (b), respectively, and in an approximately equal band intensity ratio ($I_a/I_b \approx 0.46:0.54$). As for the $\nu_7^+ \leftarrow 0^+$ band, the analysis proceeds via standard four-

TABLE 3: Available Four-Line Ground-State Combination Differences (C.D.) and Corresponding Transition Frequencies for the $\nu_{7a}^- \leftarrow 0^-$ and $\nu_{7b}^- \leftarrow 0^-$ Bands of Cyclopropyl Radical[a]

$J'K_a'K_c'$	$J''K_a''K_c''$ (1)	ν_1 (cm^{-1})	$J''K_a''K_c''$ (2)	ν_2 (cm^{-1})	C.D. (cm^{-1})	obs-pred (10^{-4} cm^{-1})
			$\nu_{7a}^- \leftarrow 0^-$			
101	211	3039.6939	111	3042.4503	2.7564	1.3
221	211	3042.8642	111	3045.6211	2.7569	−3.4
211	221	3042.2360	101	3045.4060	3.1700	6.9
111	221	3039.4898	101	3042.6606	3.1708	−1.3
202	312	3038.1876	212	3042.5123	4.3247	0.3
322	312	3042.6435	212	3046.9686	4.3250	4.0
212	322	3038.0944	202	3042.5655	4.4711	0.0
312	322	3042.4025	202	3046.8739	4.4714	−3.3
221	331	3037.9396	211	3042.8642	4.9246	−1.5
321	331	3041.9200	211	3046.8450	4.9250	2.2
312	422	3036.7732	322	3042.4025	5.6293	−4.2
432	422	3042.8694	322	3048.4992	5.6298	1.4
303	413	3036.6520	313	3042.5097	5.8576	2.3
423	413	3042.5328	313	3048.3906	5.8578	4.3
422	432	3042.1886	312	3048.2568	6.0681	−1.9
322	432	3036.5744	312	3042.6435	6.0691	8.1
533	523	3042.5972	423	3049.8460	7.2489	−6.3
413	523	3035.2246	423	3042.4737	7.2491	−4.2
523	533	3042.3819	413	3049.7654	7.3835	−2.8
423	533	3035.1492	413	3042.5328	7.3836	−2.1
432	542	3035.0855	422	3042.8694	7.7839	0.3
532	542	3041.8632	422	3049.6473	7.7840	1.1
			$\nu_{7b}^- \leftarrow 0^-$			
101	211	3039.2528	111	3042.0096	2.7568	0.4
221	211	3042.4226	111	3045.1796	2.7570	0.4
111	221	3039.0478	101	3042.2179	3.1701	−0.5
211	221	3041.7945	101	3044.9648	3.1702	1.0
212	322	3037.6600	202	3042.1313	4.4714	−0.3
312	322	3041.9711	202	3046.4426	4.4715	1.2
221	331	3037.4976	211	3042.4226	4.9250	2.5
321	331	3041.4767	211	3046.4020	4.9253	5.6
303	413	3036.2284	313	3042.0854	5.8570	−4.5
423	413	3042.1313	313	3047.9885	5.8572	−2.2

[a] There are 44 and 32 ground-state two-line combination differences observed from 71 and 58 IR transitions, respectively. The differences between the same ground-state combinations in these two bands match very well with each other within experimental uncertainty. All 46 ground-state combination differences can be well fit to a Watson asymmetric Hamiltonian (A-reduction, IIIr-representation, $\sigma = 0.00035$ cm^{-1}).

TABLE 4: Rotational Constants (in cm^{-1}) and Band Origins for All of the Ground (0^+ and 0^-) and Excited (ν_7^+, ν_{7a}^-, and ν_{7b}^-)[a] States Obtained by Separate Least-Squares Fits, as Discussed in the Text[c]

	0^+	0^-	ν_7^+	ν_{7b}^-	ν_{7a}^-
A″	0.792493(16)	0.792529(14)	0.79161(38)	0.79231(6)	0.79283(7)
B″	0.689601(16)	0.689175(14)	0.68308(32)	0.68648(5)	0.68645(6)
C″	0.43936(16)	0.43907(14)	0.43501(28)	0.43675(9)	0.43515(7)
Δ_N'' (10^{-6})	1.7(4)	1.6(3)			
Δ_{NK}'' (10^{-5})	1.8(1)	−1.9(1)			
ν_0			3040.676(3)	3042.1178(4)	3042.5586(6)
σ	0.00032	0.00035	0.012	0.0015	0.0026
ν_0^b				3042.320(6)	3042.356(6)
β^b					0.2196(5)

[a] Due to the large perturbation in vibrationally excited states, the centrifugal distortion constants are fixed to 0. [b] Unperturbed band origins and the anharmonic-coupling matrix element are obtained from a simple 2 × 2 matrix treatment. [c] The numbers in the bracket represent one standard deviation of the corresponding parameter.

line combination differences, yielding 11 and 5 four-line pairs for band (a) and band (b), respectively (see Table 3). Simulations based on fits to these transitions permit a total of 71 and 58 lines to be assigned for bands (a) and (b). A total of 44 and 32 ground-state combination differences for both of these bands are extracted. Again, nuclear spin statistics can be used to assess the tunneling symmetries of these two bands, as shown in Figure 6a,b. The data in both bands are clearly consistent with 10:6 nuclear spin weights for $K_a + K_c$ = even:odd, in agreement with the expected intensity alternation for the upper tunneling (0^-) state. Furthermore, the ground-state combination differences for both bands agree to within a standard deviation of $\sigma \approx 9$ MHz. This agreement is within experimental uncertainty and implies that both bands arise out of the *same* upper tunneling state (0^-). Thus, the spectra are indeed consistent with the anticipated $\nu_7^- \leftarrow 0^-$ band, but where the upper state is clearly split by mode mixing and intensity is shared with a near-resonant vibrational level. This splitting provides more direct evidence for intramolecular vibrational redistribution (IVR) effects in the C−H stretch manifold, which will be discussed in detail in section V.

As found for the (0^+) ground tunneling level, these (0^-) states can be fit well to a Watson Hamiltonian with a standard deviation of $\sigma \approx 10$ MHz, yielding the rotational constants listed in Table 4. This standard deviation is already comparable to our experimental precision and again consistent with essentially

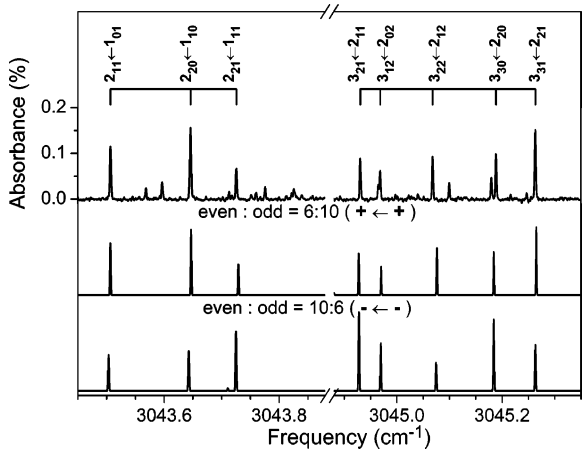

Figure 4. Comparison of the two predicted spectra with different nuclear spin weights (6:10 for the middle panel and 10:6 for the bottom panel). The band corresponding to the Q-branch in Figure 3 can be unambiguously assigned to $\nu_7^+ \leftarrow 0^+$ (nuclear spin statistics ratio is 6:10 for K_a+K_c = even:odd).

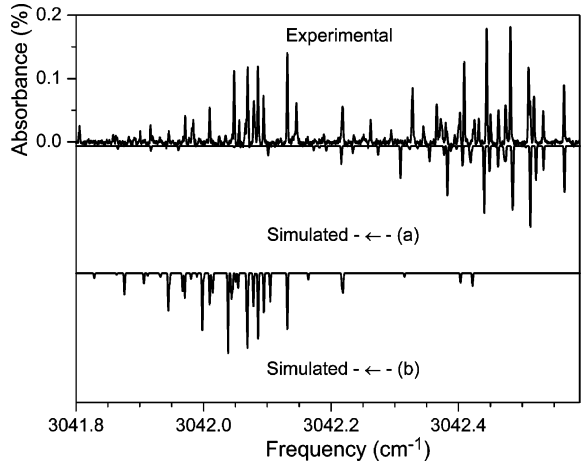

Figure 5. A second pair of Q-branches found around the predicted ν_7 stretch region of cyclopropyl radical. Both of these bands have the same nuclear spin statistics (10:6 for the K_a+K_c = even:odd) and share the same ground state (0^-), which indicates strong intramolecular-vibrational-redistribution (IVR) coupling between the ν_7^- vibrational state and one "dark" state.

completely unperturbed ground-state lower and upper tunneling levels. The two upper states, on the other hand, are both weakly perturbed and only relatively poorly fit to a rigid rotor Watson Hamiltonian, as evidenced by $\sigma \approx 200$ MHz and ≈ 170 MHz, respectively, when all lines are used in the least-squares fit. However, in contrast to what was observed in $\nu_7^+ \leftarrow 0^+$, these additional perturbations appear to be predominantly local. Specifically, by excluding all transitions to $J'K_a'K_c' = 4_{32}$ and 3_{22} levels in ν_{7a}^- (6 lines) and all transitions to $J'K_a'K_c' = 4_{23}$ and 4_{13} in ν_{7b}^- (5 lines), the fits to a rigid rotor are significantly improved, i.e., with $\sigma \approx 79$ MHz and ≈ 45 MHz (but not further improved by including centrifugal terms), respectively. The shift for these four levels is up to ≈800 MHz, which indicates the presence of local perturbations. The rotational constants and origins for both (a) and (b) bands are reported in Table 4.

From both $\nu_7^+ \leftarrow 0^+$ and $\nu_7^- \leftarrow 0^-$, the average band origin for the ν_7 fundamental vibration is ≈3041.5 cm^{-1}. This differs by only ≈3.5 cm^{-1} from the scaled B3LYP frequency predictions mentioned in section III, as indicated by the solid triangle in Figure 2. This observation demonstrates the remarkable accuracy of scaled frequency calculations in guiding high-resolution spectroscopic experiments, especially in systems

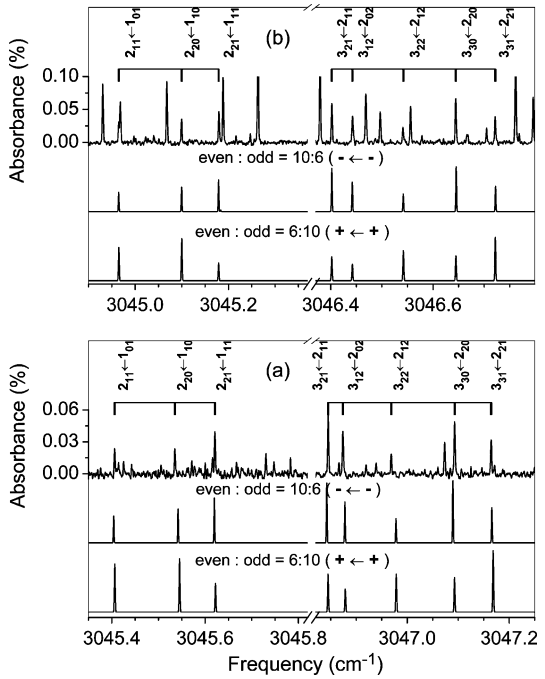

Figure 6. The assignment of two vibrational bands (Figure 5) according to the nuclear spin weights. The intensity alternation in the experimental spectra provides the nuclear spin statistics ratio to be 10:6 for the K_a+K_c = even:odd. Both bands can be assigned to $\nu_7^- \leftarrow 0^-$, indicating IVR coupling between the ν_7^- vibrational state and a nearly isoenergetic "dark" state.

where no reliable experimental assignment is available such as in the C−H stretches in vinyl radical.[62] This ν_7 band origin is also in good agreement with the only reported experimental values in Ar-matrix,[45] for which a band at 3042 cm^{-1} was observed and tentatively assigned to the ν_7 fundamental. Interestingly, an additional band at 3049 cm^{-1} was also observed in this study and assigned to ν_7. However, based on the tendency for C−H stretching vibrations in an Ar-matrix to lie below the gas-phase values[64] (typically a ≈3 cm^{-1} rms Ar-matrix-induced spectral red shift[65]), the ν_7 assignment of this blue-shifted matrix band at 3049 cm^{-1} is not consistent with our gas-phase high-resolution results.

V. Discussion

A. Cyclopropyl Radical Geometry. The agreement of the experimental intensity alternations in both the $\nu_7^+ \leftarrow 0^+$ and $\nu_7^- \leftarrow 0^-$ transitions (shown in Figures 4 and 6) implies an effective C_{2v} transition-state geometry for a cyclopropyl radical (i.e., α-CH in the CCC plane) that results from fast tunneling between equivalent C_s structures (i.e., α-CH out of the CCC plane). As the ground-state rotational constants fit the energy levels quite well, it would be interesting to extract structural information from them. Unfortunately, the cyclopropyl radical has 18 internal coordinates, which clearly cannot be determined from three rotational constants; some additional assumptions must be made to effectively reduce the problem to three degrees of freedom. First, we exploit the effective C_{2v} symmetry of the cyclopropyl radical transition state and assume the same bond lengths and angles for the two CH_2 groups. This leaves six parameters to determine the molecular structure: $r_{\alpha\beta-CC}$ and $r_{\beta\beta-CC}$ are side and base bond lengths for the isosceles CCC triangle, $r_{\alpha-CH}$ and $r_{\beta-CH}$ are the C−H bond lengths, and $\theta_{\alpha-CH}$ and $\theta_{\beta-CH}$ are the out of plane tilt angles for α-CH and β-CH moieties. Furthermore, it is empirically noted that the $r_{\alpha\beta-CC}$ and the $r_{\beta\beta-CC}$ bond lengths and the $\theta_{\beta-CH}$ bond angle have

TABLE 5: Effective Molecular Structures of Cyclopropyl Radical from Rotational Constants

	0[a]	min[b]	TS[c]	vibrationally averaged[d]
$r_{\alpha-CC}$ (Å)	1.470(1)	1.4925	1.4779	1.4909
$r_{\beta-CC}$ (Å)	1.532(1)	1.5513	1.5621	1.5527
$\theta_{\beta-CH}$	56.6(2)	57.2	57.1	57.2

[a] Since the bond length of C−H (r_{C-H}) and the tilt angle of α-CH with respect to the CCC plane ($\theta_{\alpha-CH}$) are least sensitive in the least-squares fit (maximum r_{CC} change: ≈0.004 Å per 0.01 Å change of r_{C-H} and per 10° change of $\theta_{\alpha-CH}$), they are fixed at the ab initio values, i.e., 1.09 Å for all of the r_{C-H} and 37.0° for $\theta_{\alpha-CH}$, respectively. [b,c] Geometries for the global minimum (min) and the transition state (TS) optimized at CCSD(T)/aug-cc-pVDZ. The average r_{C-H} and $\theta_{\alpha-CH}$ values are 1.096 Å and 40.4° for the minimum and r_{C-H} = 1.094 Å for the transition state. [d] With the 1D PES along the α-CH bending coordinate (calculated at CCSD(T)/aug-cc-pVDZ level), the ground-state wave function is calculated and used to evaluate vibrationally averaged bond lengths and angles.

much larger effects on the rotational constants than the remaining three structural parameters. Hence, these three less sensitive parameters are fixed to ab initio values, specifically 1.09 Å for both r_{C-H} and 37.0° for $\theta_{\alpha-CH}$, with an effective molecule structure solved by a least-squares fit to the ground-state rotational constants. Results from such fits and the ab initio predictions for the global minimum and transition-state geometries calculated at the CCSD(T)/aug-cc-pVDZ level are presented in Table 5. Despite the simplifying assumptions, the agreement between theoretical and experimental values in Table 5 is clearly very good.

In addition, vibrational averages of these three geometric quantities are reported, based on a 1D tunneling potential energy surface (PES) discussed in the next section. These vibrationally averaged geometric parameters are, in fact, quite close to those seen in the minimum energy geometry, indicating that the ground-state wave function has little amplitude near the transition state region. However, the experimentally derived C−C bond lengths are consistently shorter than predicted from ab initio calculations at either the equilibrium or transition-state geometry. This discrepancy is probably due to overestimation of the CCC ring strain at the current ab initio level, which enlarges both α-CC and β-CC bond lengths.

B. Tunneling Splittings and Inversion Barrier. Due to α-CH bending in a double minimum potential, each vibrational state in a cyclopropyl radical is split into two tunneling levels. The inversion barrier height (V_0) and the tunneling splitting (ΔE_{tun}) between these two states prove to be very important both in interpreting ESR experiments and in synthetic chemistry, since they determine the possibility of "freezing" such radicals into chiral intermediates, as the interconversion rate between the two wells can be estimated from the tunneling splitting[66] via $k_{tun} = 2\Delta E_{tun}/h$. Consequently, experimental determination of these tunneling splittings and inversion potential barriers is of considerable interest in understanding the chemical dynamics of cyclopropyl radical.

1. Thermal Extraction of Tunneling Splittings. As described in section III, the two allowed transitions, $\nu_7^+ \leftarrow 0^+$ and $\nu_7^- \leftarrow 0^-$, yield the *difference* between the upper and lower tunneling splittings of 1.6522 cm^{-1}. This difference is insufficient to yield the upper/lower tunneling splittings independently. However, we can exploit the much higher number of thermalizing 2- and 3-body collisions achieved in a linear slit geometry to extract tunneling splittings indirectly from the relative tunneling populations. This method relies on nearly complete thermal equilibrium among rotational, translational, and tunneling degrees of freedom, which has in fact been shown to be quite well satisfied in the collisionally dominated environment of the slit-jet expansion geometry. Indeed, previous studies of CO_2 containing clusters have verified thermal equilibration in the slit between rotation, translation, and intermolecular degrees of freedom with *intramolecular* vibrations as high as the ν_2 bend (≈670 cm^{-1}).[67] By way of specific example, Boltzmann analysis of HD_2O^+ molecular ions in a slit-jet expansion has been recently confirmed to be quantitatively accurate in obtaining such tunneling splittings, as tested by direct comparison with the spectroscopically determined values.[60]

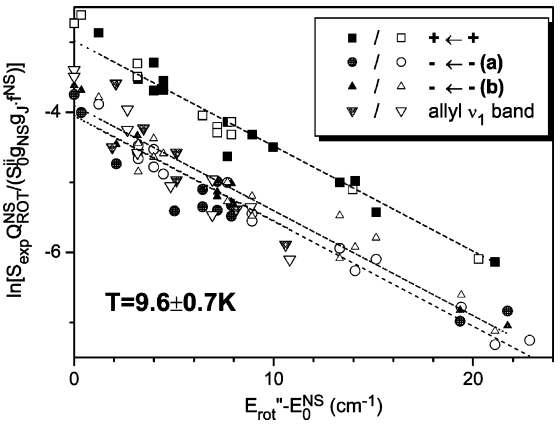

Figure 7. Boltzmann plots for $\nu_7^+ \leftarrow 0^+$ and $\nu_{7a/b}^- \leftarrow 0^-$ bands of cyclopropyl radical (dashed lines) and $\nu_1 \leftarrow 0$ of allyl radical (see text for details). Solid/unfilled symbols denote para (g_{NS}=6) and ortho states (g_{NS}=10), respectively. The linearity of the plots indicates a 9.7 ± 0.6 K rotational temperature and a fractional population of 0^-:0^+ of ≈0.73. Based on thermal equilibrium of the 0^+ and 0^- states, the inversion splittings for the ground and ν_7 excited states are estimated to be 3.2 ± 0.3 cm^{-1} and 4.9 ± 0.3 cm^{-1}, respectively.

From the direct IR absorption of rotationally resolved spectra, both the rotational temperature and the populations in the lower state can be extracted if all rotational states are in a thermal equilibrium. For a given rotational transition $j \leftarrow i$, the measured integrated line absorbance, $S_{exp} = \int A(\nu)d\nu$, is proportional to the number density of the molecules in the lower state i in the probe region (N^i), the absorption length (l = 64 cm), and the isotropically averaged line strength per M_J state (S_0^{ji}), which is given by

$$S_{exp} = N^i \cdot l \cdot S_0^{ji} = \left[N_0^{vib} \cdot f^{NS} \cdot \frac{g_{NS} \cdot g_J}{Q_{ROT}^{NS}} \cdot e^{-(E_i - E_0^{NS})/kT_{ROT}} \right] \cdot l \cdot S_0^{ji} \quad (1)$$

where N_0^{vib} is the population in the specific vibrational state vib, g_{NS} is the nuclear spin weight, g_J is the rotational degeneracy, E_0^{NS} is the lowest energy level within the same nuclear spin symmetry, and $Q_{ROT}^{NS} = g_{NS}\sum_m g_J e^{-(E_m - E_0^{NS})/kT_{ROT}}$ is the rotational partition function of a particular nuclear spin symmetry. For negligible conversion between different nuclear spin symmetries on the 1−10 μs time scale of the expansion, f^{NS} represents the fractional population of a particular nuclear spin symmetry in the stagnation region, which is either f^{NS} = 5/8 [for g_{NS} = 10 (ortho)] or f^{NS} = 3/8 [for g_{NS} = 6 (para)].

A Boltzmann analysis of the $\nu_7^+ \leftarrow 0^+$ and $\nu_{7a/b}^- \leftarrow 0^-$ bands is displayed in Figure 7, yielding plots of $\ln[S_{exp}Q_{ROT}^{NS}/(S_0^{ji} g_{NS} g_J f^{NS})]$ vs the energy difference ($E - E_0^{NS}$) between the rotational energy and the corresponding ground-state energy of the same nuclear spin symmetry. The solid symbols represent the data points from the ortho states (g_{NS} = 10), and the open symbols represent those from the para states (g_{NS} = 6). First, the linear plots for both tunneling manifolds confirm the

presence of thermal equilibrium between rotational levels within each nuclear spin symmetry manifold, corresponding to a temperature of $T_{rot} = 9.7(6)$ K. This plot further validates the efficiency of slit-jet radical/molecular ion cooling from the much higher rotational temperatures present in the discharge region. Second, the fact that the para and ortho states can be fitted to the same line indicates that the nuclear spin relaxation for the cyclopropyl radical is not an important process in the slit-jet expansion. Finally, from the intercepts of the Boltzmann plots for the three bands, the fractional population (N_0^{0-}:N_0^{0+}) between 0^- (which reflects the sum of both IVR coupled bands) and 0^+ states is found to be ≈0.73(3), making the plausible assumption that both transition line strengths are the same.

Assuming thermal equilibrium between the 0^+ and 0^- states, the energy differences between the two tunneling states (ΔE_{tun}) is proportional to the natural logarithm of the population ratio via

$$\frac{\Delta E_{tun}}{kT_{ROT}} = \ln\left(\frac{N_0^{0+}}{N_0^{0-}}\right) \qquad (2)$$

Consequently, the tunneling splittings are estimated to be $\Delta E''_{tun} = 3.2(3)$ cm^{-1} between 0^+ and 0^-, and $\Delta E''_{tun} = 4.9(3)$ cm^{-1} between the ν_7^+ and unperturbed ν_7^- states. Therefore, the inversion rate in the ground state will be ≈$2.0(4) \times 10^{11}$ s^{-1}, which is consistent with the experimentally estimated inversion rate of $10^{11}-10^{12}$ s^{-1} in the kinetic studies of cyclopropyl radical reactions.[28] With such a large tunneling contribution to the inversion rate, this interconversion will not be quenched even at a very low temperature.[28] This is consistent with EPR experiments that show hyperfine splittings for the syn and anti β-H to be approximately equal.[49]

The experimentally determined tunneling splitting is much larger than predictions for the ground state by Barone and coworkers,[40] which yield $\Delta E_{tun} \approx 1.1$ cm^{-1} and a barrier height of $V_0 \approx 1279$ cm^{-1} at the CCSD(T)/DZP level. This underpredicted tunneling splitting is almost certainly a result of overestimation of the barrier height, as confirmed by later reports from these workers of a reduced barrier height ($V_0 \approx 870$ cm^{-1}) at the CCSD(T)/DZP+ level.[36] The only previous experimental data for comparison are electron paramagnetic resonance (EPR) estimates on the substituted methyl-cyclopropyl radical, obtained by temperature-dependent Arrhenius analysis of the inversion kinetics.[22] This work yielded an empirical activation energy of 1085 (70) cm^{-1}, which, when appropriately corrected for estimated 1D zero point energy in the tunneling well, translates into an even larger barrier height of $V_0 \approx 1380(70)$ cm^{-1}. This is nearly 25% larger than the experimental values extracted herein for a cyclopropyl radical, suggesting a significant dependence of these barrier heights on ring substitution.

By way of additional confirmation, it is interesting to note that the temperatures obtained from such a rotational/tunneling Boltzmann analysis can also be compared to the translational temperature in the slit expansion, specifically derived from high-resolution Dopplerimetry from a direct absorption laser probe along the slit axis. Typical full width at half-maximum (FWHM) of the transition lines is ≈50(5) MHz (the Doppler width at room temperature is ≈176 MHz). Even without taking unresolved spin rotation and hyperfine effects into account, the FWHM due to 9.7 K thermal broadening and nonorthogonal laser beam crossings with the expansion axis would be ≈40 MHz, i.e., already in close agreement with experiment.

2. Inversion Barrier Height from 1D PES Tunneling Model. To extract the inversion barrier height from our experimental tunneling splittings, a reduced dimensionality potential energy surface (PES) has been constructed at the CCSD(T) level with an aug-cc-pVDT basis set (see Figure 8a), where all parameters have been optimized along the reaction path as a function of the α-CH tilt angle (i.e., $\theta_{\alpha-CH}$) away from the CCC plane. This 1D surface is then modified by zero-point energy (ZPE) from all vibrational modes perpendicular to the inversion coordinate. Due to finite computational resources, these frequencies are calculated at the CCSD(T) level for the global minimum and transition state geometry and then scaled to frequencies generated at the UMP2/6-311++G(3df,3pd) level to obtain a full 1D harmonic ZPE-corrected tunneling path. These ZPE effects are, in fact, relatively small, i.e., only 52 and 56 cm^{-1} differences between the global minimum and transition-state geometries are obtained at the MP2 and CCSD(T) levels, respectively. Due to the weak dependence of the high frequency vibrations on the tunneling coordinate, these differences are relatively small, with ZPE-corrected barrier heights of 956 and 926 cm^{-1}, respectively, at the CCSD(T)/aug-cc-pVDZ and MP2/6-311++G(3df,3pd) levels. The appropriately ZPE-corrected CCSD(T) 1D potentials are shown in Figure 8a.

For this double-well potential, the calculated energy levels and wave functions of the ground (0^+) and first excited (0^-) tunneling states can be obtained by numerical solution of the 1D Schrödinger equation.[68] In these calculations, the effective tunneling moment of inertia is treated explicitly as a function of the inversion coordinate, as elucidated in the work of Rush and Wiberg.[69] The ground-state-tunneling energy difference between these two states is predicted to be ≈4.3 cm^{-1} (exaggerated in Figure 8a for clarity); this is substantially larger than the experimental value of 3.2 cm^{-1}, indicating that the CCSD(T) ab initio barrier is too low. If one assumes that the correct *shape* of the inversion surface is adequately captured by the ab initio calculations, we can offer a semiempirical improvement on the barrier height predictions by (i) linearly

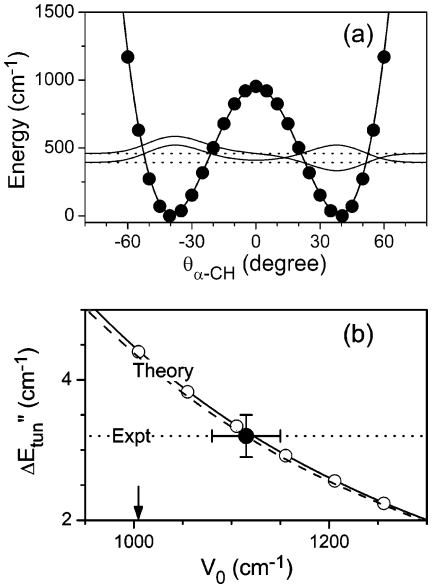

Figure 8. (a). ZPE-corrected 1D PES for cyclopropyl radical along the α-CH-bending coordinate constructed at the CCSD(T)/aug-cc-pVDZ level, with the first and second tunneling wave functions superimposed (tunneling splitting exaggerated for clarity). (b) Predicted tunneling splitting $\Delta E_{tun}''$ vs scaled inversion barrier height (V_0), where solid and dashed lines reflect harmonic and anharmonic ZPE-corrected results, respectively. By matching to the experimental tunneling splitting (3.2 ± 0.3 cm^{-1}), the inversion barrier height is estimated to be $V_0 = 1115$ ± 35 cm^{-1} (solid dot). The unscaled CCSD(T) barrier height at ($V_0 =$ 1010 cm^{-1}) is indicated by a solid arrow.

TABLE 6: Comparison of the Tunneling Splitting (ΔE_{tun}) and Inversion Barrier Height (V_0) for the Ground (0) and Excited (ν_7) States in the Cyclopropyl Radical[e]

	Barone[a]	Barone[b]	Deycard[c]	CCSD(T)[d]	expt
ΔE^0_{tun}	1.1			4.3	3.2 ± 0.3
$\Delta E^{\nu_7}_{tun}$					4.9 ± 0.3
V_0	1279	870	1340	1010	1115 ± 35

[a] Reference 40. [b] Reference 37. [c] Experimental value for 1-methylcyclopropyl (ref 22), with the Arrhenius activation energy (1068 cm^{-1}) corrected by zero-point energy in the tunneling well. [d] Calculated at CCSD(T)/aug-cc-pVDZ. [e] All units are in cm^{-1}.

scaling the 1D potentials, (ii) solving the 1D Schrödinger equation, and (iii) mapping out the predicted tunneling splittings as a function of the new barrier height. Such a curve for the ZPE-corrected CCSD(T) 1D potential is presented as the solid line through the open circles in Figure 8b, which, as expected, exhibit an *increase* in tunneling splitting with a *decrease* in scaled barrier height. At an even more subtle level, one can make additional corrections for anharmonicity effects in the ZPE calculations. Specifically, previous studies for similar molecular structures at the CCSD(T) level suggest an anharmonic scaling of the total ZPE by 0.94; this results in only a modest ($\approx$3 cm^{-1}) correction in ZPE-corrected barrier heights and thus the dashed curve in Figure 8b. A reasonable estimate of the actual barrier height, therefore, can be made by matching these curves to the experimentally measured 3.2 ± 0.3 cm^{-1} tunneling splitting (dotted line). This corresponds to an approximate inversion barrier height estimate of $V_0 = 1115 \pm 35$ cm^{-1} (represented as a solid dot in Figure 8b), where the uncertainty simply reflects the spread of results obtained with the two comparison surfaces. Although there is substantial scatter ($\approx$50%) in previous theoretical results (see Table 6), the present experimentally determined barrier is quite close ($\approx$10%) to ab initio predictions ($V_0 = 1010$ cm^{-1}) presented herein, indicating that potential surface calculations at the CCSD(T)/aug-cc-pVDZ level offer a reasonably accurate description of the tunneling dynamics.

C. IVR Anharmonic Coupling. Based on in-phase antisymmetric CH_2 stretch (ν_7) transitions out of the two tunneling states of cyclopropyl radical, only a single pair of "lower ← lower" and "upper ← upper" bands is expected. Instead, we observe *three* distinct high-resolution bands in this region. From the observed nuclear spin intensity alternation, one can unambiguously identify the lowest frequency b-type band (at $\approx$3040.68 cm^{-1}) as originating from the *lower* tunneling state, with the two higher-frequency c-type bands (at $\approx$3042.32 and 3042.35 cm^{-1}) both with nearly equal intensity and originating from the same *upper* tunneling level. This clearly implies that the excited vibrational states from these two transitions are quite closely spaced, on the order of 0.4 cm^{-1}, and strongly coupled. However, it is very unlikely that this second state results from some other fundamental or overtone excitation of cyclopropyl, since ab initio calculations indicate all other such c-type vibrational transitions to be >100 cm^{-1} away from the ν_7 stretch,[70] while experimentally, the frequency difference between these two "upper ← upper" c-type bands is less than 0.4 cm^{-1}. Furthermore, the direct IR absorption intensity from the first overtone vibration would be $\approx$50 times weaker than that of the fundamental radical transitions,[71] which would be unobservable at our current experimental sensitivity. Finally, for transitions due to tunneling splitting in both ground and excited states, there should always be at least two subbands appearing simultaneously. All these factors suggest that the third band originates from a nominally "dark" state which "borrows" intensity from the optically active "bright" state (i.e., the upper tunneling level of the ν_7 stretch) through intramolecular mode mixing in the excited state. The fact that all of the J_{KaKc}' states are split into two lines with essentially the same spacing (except for several individual states discussed later) indicates that the such mixing (often termed frequency domain IVR) must be dominated by anharmonic coupling with a dark vibrational state and should be well described by a single coupling matrix element (β).

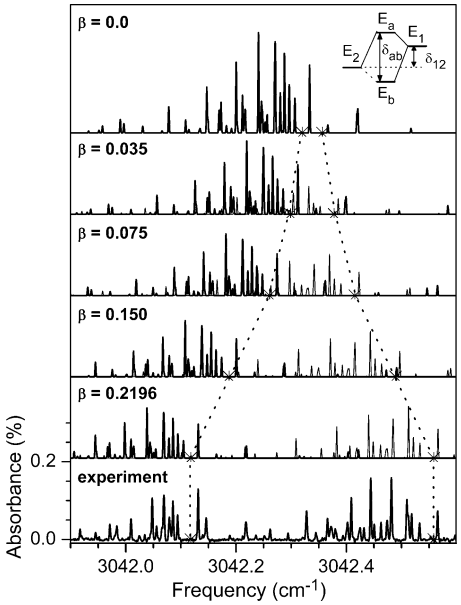

Figure 9. The two experimental Q-branches assigned to $\nu_7^- \leftarrow 0^-$ can only be quantitatively reproduced by adding an anharmonic coupling matrix element (β). The low-frequency band with more intensity (band b, while I_b:$I_a \approx 0.54$:0.46) is assumed to be the "bright" state in the fitting. As β increases, the "dark" state "borrows" more intensity from the "bright" state, and the separation between the two shifted band origins increases (as the dotted lines shown between the different panels).

With the experimental measured band intensity ratio of I_a/I_b and two perturbed energy levels, the matrix element (β) and two unperturbed energy levels can be calculated with a simple two-state model.[72] Since the "borrowed" intensity in the perturbed "dark" state is always less than or equal to the intensity from the perturbed "bright" state, the lower frequency band $\nu_{7b}^- \leftarrow 0^-$ can be nominally assigned to the "bright state". Therefore, based on a simple two-level anharmonic-coupling mechanism (see the inset in Figure 9), the matrix element (β) and the unperturbed energy levels (E_1 and E_2) can be calculated according to

$$E_{a,b} = \frac{(E_1 + E_2)}{2} \pm \frac{1}{2}[4\beta^2 + {\delta_{12}}^2]^{1/2} \quad (3)$$

$$\delta_{ab} = E_a - E_b = [4\beta^2 + {\delta_{12}}^2]^{1/2}, \text{ and} \quad (4)$$

$$\frac{I_a}{I_b} = \frac{\delta_{ab} - \delta_{12}}{\delta_{ab} + \delta_{12}} \quad (5)$$

where $\delta_{12} = E_1 - E_2$ is the energy separation between the unperturbed states. As shown in Figure 9, the larger the matrix element is, the greater the intensity spreading and the larger the energy separation between two perturbed states will be. From such a two-state modeling of the spectrum, the states are almost isoenergetic with an unperturbed separation of 0.035(6) cm^{-1} and an anharmonic coupling matrix element of 0.2196(5) cm^{-1}.

Such strong mixing of the ν_7^- vibration with some dark-coupling vibrational state (ν_{cs}) in cyclopropyl is relatively

surprising. From a direct count based on the ab initio harmonic frequencies, one predicts ≈1 state/cm^{-1} for the vibrational density of states at ≈3000 cm^{-1} of internal energy. In combination with the observed *lack* of IVR doubling for the lower-lower tunneling band, this suggests that this coupling is due to a fortuitous near resonance between ν_7 with a combination band of lower frequency modes but which tunes sufficiently out of resonance for the other symmetry tunneling state. Given sufficient information about vibrational frequencies and anharmonicities in the low-frequency modes, it could be possible to identify this state, as demonstrated by McIlroy and co-workers[70] in a study of propyne. Since this work represents the first high-resolution spectroscopic study of a cyclopropyl radical, further assignment of the coupled state would require considerably more spectroscopic information than is currently available. However, the size of the matrix element (≈0.2 cm^{-1}) is an order of magnitude larger than typically observed for C−H stretch excited states in terminal acetylenes (≈0.01 cm^{-1}), which may reflect a stronger IVR coupling for C−H stretch moieties less physically isolated from the rest of the molecular framework. From a time domain perspective, coherent excitation of both bands would result in ≈24 ps oscillation between bright and dark vibrational states,[70] which is consistent with the picosecond time-scale predictions from earlier thermal and chemical activation studies.[73,74]

In addition to the strong IVR anharmonic effects discussed above, there are some weak, but pervasive, couplings with the background states, especially the relatively large perturbations ($\beta \approx 0.03$ cm^{-1}) at the levels with $J' = 5$ in the ν_7^+ state and $J' = 4$ in both $\nu_{7a/b}^-$ and the dark states. Very few of the high J levels in ν_7^+ are observed due to the low thermal populations in the supersonic expansion, which currently precludes identification of obvious avoided crossing patterns. With the jet-cooled spectrum assigned, however, it should be possible to observe cyclopropyl radical in photolysis systems under higher temperature thermal conditions, which may be able to shed more light on this issue as well as facilitate further kinetic studies of this important combustion radical.

D. Ring Opening to Allyl Radical. With high-resolution IR detection methods, both cyclopropyl and allyl radicals can be probed simultaneously in the slit jet. As a final comment, therefore, this IR detection method can be used to test for allyl radical formation from ring opening of cyclopropyl radical as products of dissociative electron attachment with cyclopropyl halide precursor. Interestingly, although cyclopropyl radical formation clearly dominates, all three bands (ν_1, ν_2, and ν_{13}) in the C−H stretch region of an allyl radical are also observed, with a *common* rotational temperature (see Figure 7). Summing over such a Boltzmann plot permits the integrated absorbances of the ν_1 allyl and ν_7 cyclopropyl radical bands to be estimated at ≈1.2 × 10^{-5} cm^{-1} and ≈2.5 × 10^{-4} cm^{-1}, respectively. Based on ab initio integrated band strengths of 3.32 × 10^{-18} and 2.34 × 10^{-18} cm/radical for the cyclopropyl and allyl bands, respectively, this translates into a small but finite (≈7%) channel for a cyclopropyl ring opening in the discharge environment and a total density of ≈2 × 10^{12} radicals/cm^3. Such results do not exclude a direct allyl radical formation pathway from dissociative electron attachment of the cyclopropyl bromide. However, there is insufficient time in the discharge region (≈1 μs) for secondary fragmentation of the cyclopropyl radical itself at these current densities. Such pathways can be further distinguished by varying experimental conditions, in particular by discharge current and/or choice of precursor. Nevertheless, our experiment does demonstrate that a small but finite cyclopropyl ring-opening channel does occur that can be monitored via high-resolution spectroscopic methods. Furthermore, by selective precursor deuteration of the CH_2 groups, it should be possible to measure branching ratios into the resulting allyl isotopomers (i.e., syn or anti). Such studies would be able to address long standing issues concerning the detailed ring opening mechanism in a cyclopropyl radical, specifically either via a disrotatory and/or conrotatory path.

VI. Summary

High-resolution IR spectra of jet-cooled cyclopropyl radical have been recorded with the combination of high-sensitivity direct absorption methods with slit-jet discharge supersonic expansions. Three c-type bands have been observed at around 3041.5 cm^{-1}. While two bands can be assigned to the ν_7 band (in-phase antisymmetric CH_2 stretch) of a cyclopropyl radical due to the α-CH inversion (two allowed vibrational transition bands $\nu_7^+ \leftarrow 0^+$ and $\nu_7^- \leftarrow 0^-$), the third band comes from the anharmonic coupling between ν_7^- and an nearly isoenergetic "dark" state with the matrix element $\beta \approx 0.2196$ cm^{-1}. With the reasonable assumption of thermal equilibrium between the 0^+ and 0^- states, tunneling splittings for the ground and ν_7 excited states are estimated to be 3.2 ± 0.3 cm^{-1} and 4.9 ± 0.3 cm^{-1}, respectively, which, in particular, translates into a 2.0(4) × 10^{11} s^{-1} α-CH inversion rate for the ground state. In addition to band origins and rotational constants obtained from the least-squares fit of high-resolution data to an A-reduction Watson asymmetric top rotor Hamiltonian, the first precise gas-phase structural information on a cyclopropyl radical has also been reported. In contrast with the high quality least-squares fits observed to the *ground-state* combination differences, the *upper-state* discrepancies between observed and calculated for some rotational levels suggest weak but pervasive perturbations in the upper states. Furthermore, the inversion barrier height has been estimated from the experimental tunneling splitting to be $V_0 = 1115 \pm 35$ cm^{-1} in the ground state. Finally, direct evidence for a weak but finite ring-opening channel (≈7%) in the formation of a cyclopropyl radical is observed by simultaneous IR detection of an allyl radical in the slit-jet expansion.

Acknowledgment. This work has been supported by grants from the National Science Foundation and the Air Force Office of Scientific Research. D.J.N. would also like to take the opportunity to thank Professor Juergen Troe for his ever thoughtful friendship, his excellent baritone singing, and a truly inspirational lifelong passion for science.

References and Notes

(1) Anderson, J. G. *Annu. Rev. Phys. Chem.* **1987**, *38*, 489.
(2) Olah, G. A.; Molnar, A. *Hydrocarbon Chemistry*; John Wiley & Sons: New York, 1995.
(3) Miller, J. A.; Kee, R. J.; Westbrook, C. K. *Annu. Rev. Phys. Chem.* **1990**, *41*, 345.
(4) Patten, T. E.; Matyjaszewski, K. *Adv. Mater.* **1998**, *10*, 901.
(5) Herbst, E. *Annu. Rev. Phys. Chem.* **1995**, *46*, 27.
(6) Herr, K. C.; Pimentel, G. C. *Appl. Opt.* **1965**, *4*, 25.
(7) Tan, L. Y.; Winer, A. M.; Pimentel, G. C. *J. Chem. Phys.* **1972**, *57*, 4028.
(8) Kanamori, H.; Endo, Y.; Hirota, E. *J. Chem. Phys.* **1990**, *92*, 197.
(9) Pacansky, J.; Dupuis, M. *J. Am. Chem. Soc.* **1982**, *104*, 415.
(10) Maltsev, A. K.; Korolov, V. A.; Nefedov, O. M. *Bull. Acad. Sci. USSR, Div. Chem. Sci.* **1982**, *31*, 2131.
(11) Morter, C. L.; Domingo, C.; Farhat, S. K.; Cartwright, E.; Glass, G. P.; Curl, R. F. *Chem. Phys. Lett.* **1992**, *195*, 316.
(12) Tan, X. Q.; Wright, T. G.; Miller, T. A. *Jet Spectroscopy and Molecular Dynamics*; Blackie Academic and Professional: London, 1995.
(13) Davis, S.; Anderson, D. T.; Duxbury, G.; Nesbitt, D. J. *J. Chem. Phys.* **1997**, *107*, 5661.

(14) Sears, T. J.; Johnson, P. M.; Jin, P.; Oatis, S. *J. Chem. Phys.* **1996**, *104*, 781.
(15) Davis, S.; Uy, D.; Nesbitt, D. J. *J. Chem. Phys.* **2000**, *112*, 1823.
(16) Han, J. X.; Utkin, Y. G.; Chen, H. B.; Hunt, N. T.; Curl, R. F. *J. Chem. Phys.* **2002**, *116*, 6505.
(17) Uy, D.; Davis, S.; Nesbitt, D. J. *J. Chem. Phys.* **1998**, *109*, 7793.
(18) Sumiyoshi, Y.; Imajo, T.; Tanaka, K.; Tanaka, T. *Chem. Phys. Lett.* **1994**, *231*, 569.
(19) Brown, H. C.; Fletcher, R. S.; Johannesen, R. B. *J. Am. Chem. Soc.* **1951**, *73*, 212.
(20) Fessenden, R. W.; Schuler, R. H. *J. Chem. Phys.* **1963**, *39*, 2147.
(21) Beckwith, A. L. J.; Bowry, V. W. *J. Am. Chem. Soc.* **1994**, *116*, 2710.
(22) Deycard, S.; Hughes, L.; Lusztyk, J.; Ingold, K. U. *J. Am. Chem. Soc.* **1987**, *109*, 4954.
(23) Dyke, J.; Ellis, A.; Jonathan, N.; Morris, A. *J. Chem. Soc., Faraday Trans. 2* **1985**, *81*, 1573.
(24) Greig, G.; Thynne, J. C. J. *Trans. Faraday Soc.* **1966**, *62*, 3338.
(25) Greig, G.; Thynne, J. C. J. *Trans. Faraday Soc.* **1967**, *63*, 1369.
(26) Johnston, L. J.; Scaiano, J. C.; Ingold, K. U. *J. Am. Chem. Soc.* **1984**, *106*, 4877.
(27) Johnston, L. J.; Lusztyk, J.; Wayner, D. D. M.; Abeywickreyma, A. N.; Beckwith, A. L. J.; Scaiano, J. C.; Ingold, K. U. *J. Am. Chem. Soc.* **1985**, *107*, 4594.
(28) Johnston, L. J.; Ingold, K. U. *J. Am. Chem. Soc.* **1986**, *108*, 2343.
(29) Nandi, S.; Arnold, P. A.; Carpenter, B. K.; Nimlos, M. R.; Dayton, D. C.; Ellison, G. B. *J. Phys. Chem. A* **2001**, *105*, 7514.
(30) Seburg, R. A.; Squires, R. R. *Int. J. Mass Spectrom. Ion Process* **1997**, *167*, 541.
(31) Walborsky, H. M.; Ollman, J.; Hamdouchi, C.; Topolski, M. *Tetrahedron Lett.* **1992**, *33*, 761.
(32) Walborsky, H. M. *Tetrahedron* **1981**, *37*, 1625.
(33) Sustmann, S.; Ruchardt, C.; Boche, G.; Bieberba, A. *Tetrahedron Lett.* **1972**, 4759.
(34) Arnold, P. A.; Cosofret, B. R.; Dylewski, S. M.; Houston, P. L.; Carpenter, B. K. *J. Phys. Chem. A* **2001**, *105*, 1693.
(35) Barone, V.; Grand, A.; Minichino, C.; Subra, R. *J. Chem. Phys.* **1993**, *99*, 6787.
(36) Barone, V.; Adamo, C.; Brunel, Y.; Subra, R. *J. Chem. Phys.* **1996**, *105*, 3168.
(37) Barone, V.; Subra, R. *J. Chem. Phys.* **1996**, *104*, 2630.
(38) Dupuis, M.; Pacansky, J. *J. Chem. Phys.* **1982**, *76*, 2511.
(39) Olivella, S.; Sole, A.; Bofill, J. M. *J. Am. Chem. Soc.* **1990**, *112*, 2160.
(40) Barone, V.; Minichino, C.; Faucher, H.; Subra, R.; Grand, A. *Chem. Phys. Lett.* **1993**, *205*, 324.
(41) Limbach, M.; Dalai, S.; De Meijere, A. *Adv. Synth. Catal.* **2004**, *346*, 760.
(42) Arnold, P. A.; Carpenter, B. K. *Chem. Phys. Lett.* **2000**, *328*, 90.
(43) Mann, D. J.; Hase, W. L. *J. Am. Chem. Soc.* **2002**, *124*, 3208.
(44) Szeimies, G.; Boche, G. *Angew. Chem., Int. Ed. Engl.* **1971**, *10*, 912.
(45) Holtzhauer, K.; Comettamorini, C.; Oth, J. F. M. *J. Phys. Org. Chem.* **1990**, *3*, 219.
(46) Hoffmann, R.; Woodward, R. B. *J. Am. Chem. Soc.* **1965**, *87*, 395.
(47) Longuet-Higgins, H. C.; Abrahamson, E. W. *J. Am. Chem. Soc.* **1965**, *87*, 2045.
(48) Boche, G.; Szeimies, G. *Angew. Chem., Int. Ed. Engl.* **1971**, *10*, 911.
(49) Kochi, J. K.; Bakuzis, P.; Krusic, P. J. *J. Am. Chem. Soc.* **1973**, *95*, 1516.
(50) Desain, J. D.; Thompson, R. I.; Sharma, S. D.; Curl, R. F. *J. Chem. Phys.* **1998**, *109*, 7803.
(51) Desain, J. D.; Sharma, S. D.; Curl, R. F. *Abstr. Pap. Am. Chem. Soc.* **1998**, *215*, U231.
(52) Desain, J. D.; Curl, R. F. *J. Mol. Spectrosc.* **1999**, *196*, 324.
(53) Lovejoy, C. M.; Nesbitt, D. J. *J. Chem. Phys.* **1987**, *86*, 3151.
(54) Davis, S.; Farnik, M.; Uy, D.; Nesbitt, D. J. *Chem. Phys. Lett.* **2001**, *344*, 23.
(55) Anderson, D. T.; Davis, S.; Zwier, T. S.; Nesbitt, D. J. *Chem. Phys. Lett.* **1996**, *258*, 207.
(56) Riedle, E.; Ashworth, S. H.; Farrell, J. T.; Nesbitt, D. J. *Rev. Sci. Instrum.* **1994**, *65*, 42.
(57) Pine, A. S. *J. Opt. Soc. Am.* **1976**, *66*, 97.
(58) Bunker, P. R.; Jensen, P. *Molecular Symmetry and Spectroscopy*, 2nd ed.; NRC Research Press: Ottawa, 1998.
(59) Dong, F.; Nesbitt, D. J. Manuscript in preparation.
(60) Dong, F.; Uy, D.; Davis, S.; Child, M.; Nesbitt, D. J. *J. Chem. Phys.* **2005**, *122*, 224301.
(61) Whitney, E. S.; Dong, F.; Nesbitt, D. J. Manuscript in preparation.
(62) Dong, F.; Nesbitt, D. J. Manuscript in preparation.
(63) Davis, S.; Uy, D.; Kable, S. H.; Nesbitt, D. J. *Abstr. Pap. Int. Sym. Mol. Spectrosc.* **1998**, WH07.
(64) Jacox, M. E. *Chem. Phys.* **1994**, *189*, 149.
(65) Huneycutt, A. J.; Casaes, R. N.; Mccall, B. J.; Chung, C. Y.; Lee, Y. P.; Saykally, R. J. *Chem. Phys. Chem.* **2004**, *5*, 321.
(66) Eyring, H.; Walter, J.; Kimball, G. E. *Quantum Chemistry*; Wiley: New York, 1954.
(67) Lovejoy, C. M.; Schuder, M. D.; Nesbitt, D. J. *J. Chem. Phys.* **1987**, *86*, 5337.
(68) Levine, I. N. *Quantum Chemistry*, 5th ed.; Prentice Hall: Upper Saddle River, NJ, 2000.
(69) Rush, D. J.; Wiberg, K. B. *J. Phys. Chem. A* **1997**, *101*, 3143.
(70) Mcilroy, A.; Nesbitt, D. J. *J. Chem. Phys.* **1989**, *91*, 104.
(71) Lehmann, K. K.; Smith, A. M. *J. Chem. Phys.* **1990**, *93*, 6140.
(72) Herzberg, G. *Infrared and Raman Spectra of Polyatomic Molecules*; D. Van Nostrand Company, Inc.: New York, 1946; Vol. II.
(73) Larson, C. W.; Rabinovitch, B. S. *J. Chem. Phys.* **1961**, *51*, 2293.
(74) Tandy, D. C.; Larson, C. W.; Rabinovitch, B. S. *Can. J. Chem.* **1968**, *46*, 6, 341.